NATIONAL RADIO ASTRONOMY OBSERVATORY
GREEN BANK, WEST VIRGINIA

ELECTRONICS DIVISION INTERNAL REPORT NO. 240

L-BAND RECEIVER:
INITIAL TESTS AT 18 cm AND 21 cm

H. E. PAYNE

DECEMBER 1983

NUMBER OF COPIES: 150

L-BAND RECEIVER
INITIAL TESTS AT 18 cm AND 21 cm

H. E. Payne

TABLE OF CONTENTS

L-Band Receiver
Initial Tests at 18 cm and 21 cm

H.E. Payne
12 December 1983

1. Introduction

This report summarizes the results from three observing sessions with the new L-band receiver: (1) an 18 cm run on the 140' from 19 August to 23 August 1983, and 25 August to 1 September 1983, (2) a 21 cm run on the 140' from 13 September to 19 September 1983, and (3) a 21 cm run on the 300' from 20 September to 26 September 1983. Some supplementary data were obtained during gaps in the 18 cm VLBI run between 14 October and 21 October 1983. These runs were intended to provide pointing for the new feeds, along with some basic calibration data. The runs on the 140' were also used for initial observations in the spectral line mode, including the compilation of an atlas of bandpass shapes and baselines from total power observations of continuum sources. Tests for stability and sensitivity, mostly involving observations of known weak lines were enthusiastically performed by B.E. Turner for the 18 cm feed and F.J. Lockman for the 21 cm feed.

All of the continuum data obtained for pointing and calibration were obtained with the digital continuum receivers (DCR) in the total power mode, meaning that all of the calibration factors to be applied to the raw power counts are continuously updated by the DCR between scans, with the last determined factors applied throughout the following scan, observed with the calibration noise source turned off. System temperatures read from the DCR do not include a contribution from the cal. In most places in this report the system temperatures have been increased by one half of the cal value to reflect the system temperature appropriate for spectral line observing.

All of the continuum observations were made in linear polarization with a box rotation of 0°. In this configuration the E-field in channel A is aligned east-west, and the E-field in channel B is aligned north-south. A 12 MHz bandwidth filter centered on the IF of 250 MHz was used for all of the continuum observations. To determine frequency dependent effects the ULO was set to center the desired frequency band on the 250 MHz IF. The bandpass filter kept the interferometer link out of the 21 cm observations except for a band centered on 1355 MHz. Focus and pointing data were obtained for channel A only.

The 140' observations are reported first since there it is possible to measure most quantities of interest much more conveniently. These observations serve as a guide to effects which were only spot checked at the 300'. In particular, determining the focus as a function of frequency at the 300' was not very successful, and beam maps were not attempted.

2. 140' Observations

2.1. Pointing

Pointing data well distributed in the hour angle - declination plane were obtained at both 21 cm and 18 cm. Feed offsets between the two sets of data were so small that the two sets could be combined into a single data set consisting of approximately 550 usable data points. Fits were made to the 11 parameter pointing equations suggested by von Hoerner and long in use at the 140', and to the 12 parameter equations involving the addition of an ad hoc 12th term to the above. The 12th term, affecting only the hour angle pointing, was inserted into the pointing corrections for the cassegrain system in September 1982 to improve the pointing at the highest frequencies.

The results of both fits are summarized in Table 1. The effect of small feed offsets is confined to coefficients 1, 6, and 8. It is these terms which are corrected with PVALS at the telescope. It can be seen from Table 1 that the new 11 parameter fit is not significantly different from the old 11 parameter fit, except for a declination offset. With the new 11 parameter fit, the rms pointing error was 10" in declination and 18" in right ascension. With the 12 parameter fit the rms pointing error was reduced to 9" in declination and 13" in right ascension. The fitting program decides which data points to reject, and these rms values apply to the filtered data. Empirical rules for assessing the reliability of a particular pointing measurement are given below. The statistical significance of the 12th coefficient in the fit to these prime focus data is very high.

As described in detail elsewhere, the program for determining the pointing coefficients from a set of pointing observations has undergone two significant revisions. The first is the addition of an ad hoc 12th term, motivated by an examination of pointing errors in the cassegrain system at an observing wavelength of 1.3 cm. As just mentioned, this 12th term significantly improves the fit at prime focus as well. The second change is in the fitting algorithm. As a first step, the program now performs a least-sum fit to the data. That is, the sum of the absolute values of the residuals is minimized. Since bad measurements are not squared, this fit is less susceptible to contamination by bad data points. This first fit is then used to find the highly discrepant points and filter them out, so that the subsequent least-squares fit is free from the effect of bad data. The distribution of the residuals of the L-band pointing measurements with respect to the initial fit determined by the least sum fit is shown in Figure 1. The histograms show the hour angle and declination residuals separately. The residuals are binned in units of the mean of the absolute value of the deviation (MAD) from the fit. The MAD values are 10".65 in declination and 15".89 in hour angle. The two outermost bins include all of the points that would fall outside the plotted region. In each histogram, the error distribution is symmetric and roughly gaussian, and therefore likely to be the result of random errors. All points within the range ±2 are passed to the least squares fit to derive the final results.

Since the program decides which data points to reject, an examination of the rejected data gives a guide to the reliability of pointing data. This is especially useful for measuring PVALS, since a small number of points is usually taken. Examination yields these empirical rules:

> An L-band pointing measurement for PVALS should be rejected if:
>
> 1) you do not see the source in the scan, any of the four printed widths or heights is wildly different from the others, or any other obvious deficiency,
>
> 2) the elevation is less than 10° for any source, if the elevation is less than 20° for all but the strongest sources, and if the elevation is less than 30° for a weak source,
>
> 3) if the two beamwidths measured by the right ascension scans differ by more than 10%,
>
> 4) if the two beamwidths measured by the declination scans differ by more than 10%,
>
> 5) if the average of the two heights measured by the dec scans is more than 10% lower than the average of the two heights measured by the right ascension scans, or
>
> 6) if the average of the two heights measured by the dec scans is more than 1/3 higher than the average of the two heights measured by the right ascension scans.

2.2. 21 cm Observations

2.2.1. 21 cm focus versus frequency

Measured values of the nominal focus as a function of frequency are shown in Figure 2. Measurements refer only to channel A. The focus was determined by the operator at each frequency in the usual way, which is to peak up on a strong continuum source, to record the total power versus focus on the strip chart and then determine the midpoint between two focus settings equally far down on the steep part of this curve. The measurements are repeatable to about ±1 mm. The source 3C 295 was used for these measurements. The solid curve in the figure is not a fit to the data but simply a smooth curve drawn through the points. The figure is intended only to show the trend of focus versus frequency since the focus should be checked for the frequency and bandwidth of a particular observation.

2.2.2. 21 cm system temperature at zenith versus frequency

The system temperature at zenith as a function of frequency is shown in Figure 3. The system temperature in each channel varies by ±2 K or roughly 8% across the observed frequency range. The system temperatures shown include one half of the cal value, as appropriate for spectral line observations. The cal values are shown if temperatures appropriate to total power continuum observations are desired. The frequency of galactic HI lies near the minimum system temperature in both channels.

2.2.3. 21 cm aperture efficiency versus frequency

The aperture efficiency η_A is computed from the relationship between flux density S and antenna temperature T_A for a point source:

$$\eta_A = (2k/ A)*(T_A/S),$$

where k is Boltzmann's constant and A is the physical aperture of the telescope. For the 140', 2k/A is 1.930. The aperture efficiency as a function of frequency is shown in Figure 4. The measurements are derived from observations of 3C 295, assuming the spectrum fitted by Baars et al. (1977, Astron.Astrophys. 61, 99), and assuming that there is no variation in aperture efficiency with hour angle. Antenna temperatures were derived from declination scans through the source as part of the peaking up procedure, after the proper focus had been determined. These aperture efficiencies are accurate to ±0.005 or better, but will vary with frequency and bandwidth. An aperture efficiency of 0.58 corresponds to a gain of 0.30 K/Jy.

The shapes of the curves in Figure 4 closely mimic those of system temperature versus frequency. In particular, galactic HI falls near the minimum efficiency. That the efficiency rises toward the edges of the feed bandpass may indicate a mismatch. The sensitivity to a point source, computed as the ratio of aperture efficiency to system temperature, is shown as a function of frequency in Figure 5. This ratio is independent of the assumed cal value, and since this figure is aimed at continuum observers, the system temperatures used do not include a cal contribution. There is little variation across the band but channel B is about 15% less sensitive than channel A across most of the band. For the 140', if the ratio of aperture efficiency to system temperature equals 0.025, then the time-bandwidth product necessary for a one sigma detection of a one Jy source is 6000. An equivalent statement is that the difference between two ten second integrations, on and off a weak continuum source with a 20 MHz bandwidth, gives a flux density measurement with three sigma errors of 23 mJy.

2.3. 18 cm observations

2.3.1. 18 cm focus versus frequency

The variation of nominal focus with frequency at 18 cm is shown in Figure 6. These measurements were made in an identical manner to those at 21 cm, even to the point of being measured on the same source. In particular, only channel A was measured, and the solid curve in the figure is not a fit but simply a smooth curve drawn through the data.

2.3.2. 18 cm system temperature at zenith versus frequency

The system temperature at zenith as a function of frequency at 18 cm is shown in Figure 7. The system temperatures shown include half the cal value. Channel B shows a larger variation across the band, about ±2.5 K or ±10%.

2.3.3. 18 cm aperture efficiency versus frequency

The aperture efficiency at 18 cm shows little variation with frequency, as shown in Figure 8, except for a decrease at the high frequency edge of the band. Both curves vary around a value near 58%. That the system temperature and aperture efficiency versus frequency curves are not as smooth as those at 21 cm may reflect larger uncertainties in the cal values. The cal value independent ratios of aperture efficiency to system temperature (without a cal contribution) are shown in Figure 9, and are quite smooth. At the OH main line frequency, channel B is about 10% more sensitive to a point source.

2.3.4. 18 cm beam maps

Beam maps were made at a frequency of 1660 MHz, with a bandwidth of 12 MHz. Two contour maps, Figures 10 and 11, show the inner sidelobe structure measured against the very strong continuum source 3C 274. Contours are plotted at 2 db intervals. The vertical bar in the figures is 1° in length. Scans across the source were spaced by 9', and 10 scans were used to obtain the figures shown. The contour plotting routine only compares neighboring scans, rather than fitting a surface through the data, and this gives rise to the horizontal edges which appear in the figures. The sidelobes form a cloverleaf pattern along diagonals through the field. The sidelobes are about 18 db down from the peak of the main beam, and are separated by about 28' from the peak of the main beam. A weak plateau joining the two northern sidelobes, and another joining the two southern sidelobes is found in channel A. In channel B the plateaus are in the east-west directions. The positions of the sidelobes themselves are not very different between the two channels. In channel A the main beam measures about 19.1' EW by 16.8' NS, so that the main beam is narrower in the directions where the plateaus are evident. In channel B the main beam measures about 17.0' EW by 19.0' NS.

3. 300' 21 cm Observations

3.1. Focus versus frequency

An attempt to confirm the focus versus frequency behavior observed on the 140' was not very successful. I sought that focus which minimized the east-west half-power beamwidth measured by drift scans across point sources within about 25° of the zenith. The first measurements were at 1405 MHz, and gave -305 mm in channel A and -380 mm in channel B. The accuracy of these measurements is perhaps ±25 mm, poor compared to the 140'. The channel B data seemed somewhat better, so a compromise of -360 mm was used for the pointing run. Measurements at 1365 MHz and 1385 MHz gave about the same results. The data at 1425 MHz were poor and the results inconclusive.

Measurements by R. Giovanelli and M. Haynes in November 1983, again only in channel A, do confirm the trend measured on 140' over the range of 1370 to 1400 MHz. Their measurements would indicate that the best focus at the 300' is roughly 740 mm lower than shown in Figure 2.

3.2. Declination pointing

Declination pointing coefficients were obtained in the typical manner described in the 300' Telescope Observer's Manual. Observations were made by tracking a source in right ascension while scanning in declination at a rate of ±15'/min. A source list covering the declination range of the telescope was compiled from the calibration source list in the 300' manual. Each source was observed twice, scanned from north to south on one day, and scanned from south to north on the other to remove the effect of any time constants.

As a first step in the data reduction, the electronic level reading versus declination was checked. No change in the level curve was detected. The level curve coefficients were last updated on 20 August 1983, five weeks before these tests. New curves were then fit to the measured pointing offsets. As in the past, a third order polynomial in declination, fit to data corrected for deviations from the expected level reading, was used. The new coefficients are here compared to the old 21 cm pointing coefficients:

	New Coefficients		Old Coefficients
C0	-156.80	± 2.80	-214.05
C1	3.91	± 0.17	3.91
C2	0.0273	± 0.0080	0.0282
C3	-0.000283	± 0.000082	-0.000311

The table shows that the only significant change in the pointing of the new 21 cm receiver is an offset in declination. The new coefficients have been installed at the telescope as the 21 cm pointing curve coefficients.

3.3. System temperature at zenith versus frequency

The variation of system temperature at zenith with frequency is shown in Figure 12. The shape of the dependence for each receiver is similar to that found on the 140', shown in Figure 3. Note, however, that the range of plotted temperatures in Figure 12 is 10 K to 40 K, in contrast to 0 K to 30 K in Figure 3. The system temperature in channel A is roughly 9 K higher than measured on the 140' in the middle of the feed bandwidth, and the system temperature in channel B is roughly 5 K higher. The behavior at the edges of the feed bandwidth is slightly different. Especially noticeable is a large increase in the system temperature for channel A at 1435 MHz.

Giovanelli and Haynes measured the system temperature during the November 1983 installation and found much lower values, about 23 K, assuming a slightly smaller aperture efficiency, resulting in slightly smaller cal values. Using the cal values measured in the lab, as during my tests, would give temperatures around 25 to 26 K. The system temperatures were determined from spectral line observations with a 10 MHz bandwidth. During the November installation, R. Norrod measured 27 to 29 K, using the DCR and adding one half of the cal. It appears that the discrepancy between these system temperatures and those I measured earlier is due to a change in the receiver between installations. The cal values measured in the lab did not change between the two installations.

3.4. System temperature versus declination

The system temperature data shown in Figure 13 were obtained by scanning the telescope in declination, recording the system temperature calculated by the DCR on the chart recorder. Declination marks were put on the record. The data shown are actually a composite of two such scans, widely separated in time, one of which saw the galactic plane at high declinations, and the other of which saw the galactic plane at low declinations. There was, however, an offset of about 1 K between the two scans, perhaps due to an error in setting up the chart recorder. Also, the measured points need to be raised by about 1.2 K to intersect the system temperature versus frequency curves of Figure 12.

3.5. Aperture efficiency versus declination

As described above, the aperture efficiency η_A can be determined from antenna temperature measurements of point sources with known flux density. Antenna temperatures were determined from drift scans across a set of sources spanning the declination range of the 300'. Source positions and fluxes were taken from an Appendix to the 300' Telescope Observer's Manual. The ratio (2k/A) is 0.4203 for the 300'. The results for channel A are shown in Figure 14, and those for channel B are shown in Figure 15. In each case the solid curve is the best fit quadratic polynomial in declination. To allow comparison, the two fits are shown together in Figure 16. The top curve is channel B. The two fits are:

Channel A: $\eta_A = 0.434 + 0.00430*\delta - 0.0000565*\delta^2$

Channel B: $\eta_A = 0.499 + 0.00289*\delta - 0.0000431*\delta^2$

In contrast to observations on the 140', the aperture efficiency is higher in channel B than in A. The peak efficiency in each channel is lower than it is on the 140'. On the 300', an aperture efficiency of 0.54 corresponds to a gain of 1.28 K/Jy.

3.6. Beamwidth versus declination

Since beam mapping is quite tedious on the 300', the only convenient measure of the beam shape is the half-power width of the main beam obtained by scans across the source. North-south scans used for declination pointing and east-west drift scans used for aperture efficiency measurements provide a large sample of such data. The results for channel A are shown in Figures 17 and 18 and the results for channel B are shown in Figures 19 and 20. Above 10° of declination all four curves are flat, yielding beam shapes of 9.6' EW by 10.4' NS for channel A and 8.9' EW by 11.3' NS for channel B. The beam in channel A degrades at declinations below 10°, as confirmed by the more rapid loss of aperture efficiency shown in Figure 16.

3.7. Aperture efficiency versus hour angle

Aperture efficiency as a function of hour angle was something that we were able to measure, using the DCR and the strip chart recorder, while the off-line computer was down. While tracking in hour angle, the operator (R. Davis -- thanks Rick) dialed in a declination rate to drive alternately north and south across the source while I used a battery and a switch to put hour angle marks on the strip chart. By measuring the height and position of the peaks in the resultant strip chart record the antenna temperature, and therefore aperture efficiency as a function of hour angle can be determined. The tracking in hour angle was slow enough that any time delay in the detectors and recorders was negligible. We made measurements on a single receiver channel at a time. For each channel we tracked two sources, fortuitously at roughly symmetrical positions on the aperture efficiency versus declination curves. The results are shown in Figure 21 for channel A and Figure 22 for channel B. As better shown in Figure 22, the aperture efficiency at the travel limits of the Sterling mount drops to about 85% of its on axis value.

3.8. Sample results

To demonstrate the properties of the receiver during actual observations, I observed a small subset of the Tully-Fisher sample of galaxies. The recent compilation of spectra from their survey served as a basis for comparison. Sample results for NGC 7331, NGC 7721, and NGC 7218 are shown in Figures 23 to 25. Each of these galaxies was observed with a 10 MHz bandwidth. Total power off scans were obtained both before and after the on source scan, and were averaged together.

The results shown are the average of both polarizations. A linear baseline has been removed, but there was very little slope in the raw baseline, as well as no noticeable curvature. A cal value of 4.00 K was used for all of the observations, which is an overestimate. In the figures, heliocentric velocity is shown on the horizontal scale.

Table 1

140' Prime Focus Pointing Corrections
Derived from 21 cm and 18 cm Observations

Coefficient	Declination term	Hour Angle term	Old 11 Param fit	New 11 Param fit	New 12 Param fit
C(1)	1.0		2.14	1.75 ± 0.04	1.74 ± 0.03
C(2)	sin(h)		-0.51	-0.56 ± 0.02	-0.61 ± 0.02
C(3)	cos(h)		-2.22	-2.09 ± 0.05	-2.07 ± 0.04
C(4)	sin(δ)*cos(h)-tan(l)*cos(δ)		0.86	0.85 ± 0.05	0.85 ± 0.04
C(5)	Q*(sin(l)-sin(δ)*cos(z)/cos(δ))	-Q*cos(l)*cos(h)	0.98	1.03 ± 0.02	1.03 ± 0.01
C(6)		1.0	-1.65	-1.64 ± 0.09	-1.80 ± 0.07
C(7)		sin(δ)	-0.47	-0.43 ± 0.04	-0.61 ± 0.03
C(8)		cos(δ)	1.17	1.40 ± 0.10	1.19 ± 0.08
C(9)		sin(h)	-0.15	0.16 ± 0.18	-0.30 ± 0.14
C(10)		sin(δ)*sin(h)	-0.30	-0.15 ± 0.09	-0.09 ± 0.07
C(11)		cos(δ)*sin(h)	0.04	-0.39 ± 0.17	0.09 ± 0.13
C(12)		cos(z)*cos(h)			0.76 ± 0.04

Hour angle terms are actually fit to (hour angle offset)*cos(δ) to avoid over weighting points observed near the pole.
δ = declination, h = hour angle, z = zenith distance, l = latitude of 140' = 38° 26' 15.″396
Q = K / (cos(z) + 0.00175*tan(z-2.°5)), where K, a measured quantity, is a weather-dependent correction of the refraction term (von Hoerner, NRAO E.D.I.R. no. 101)

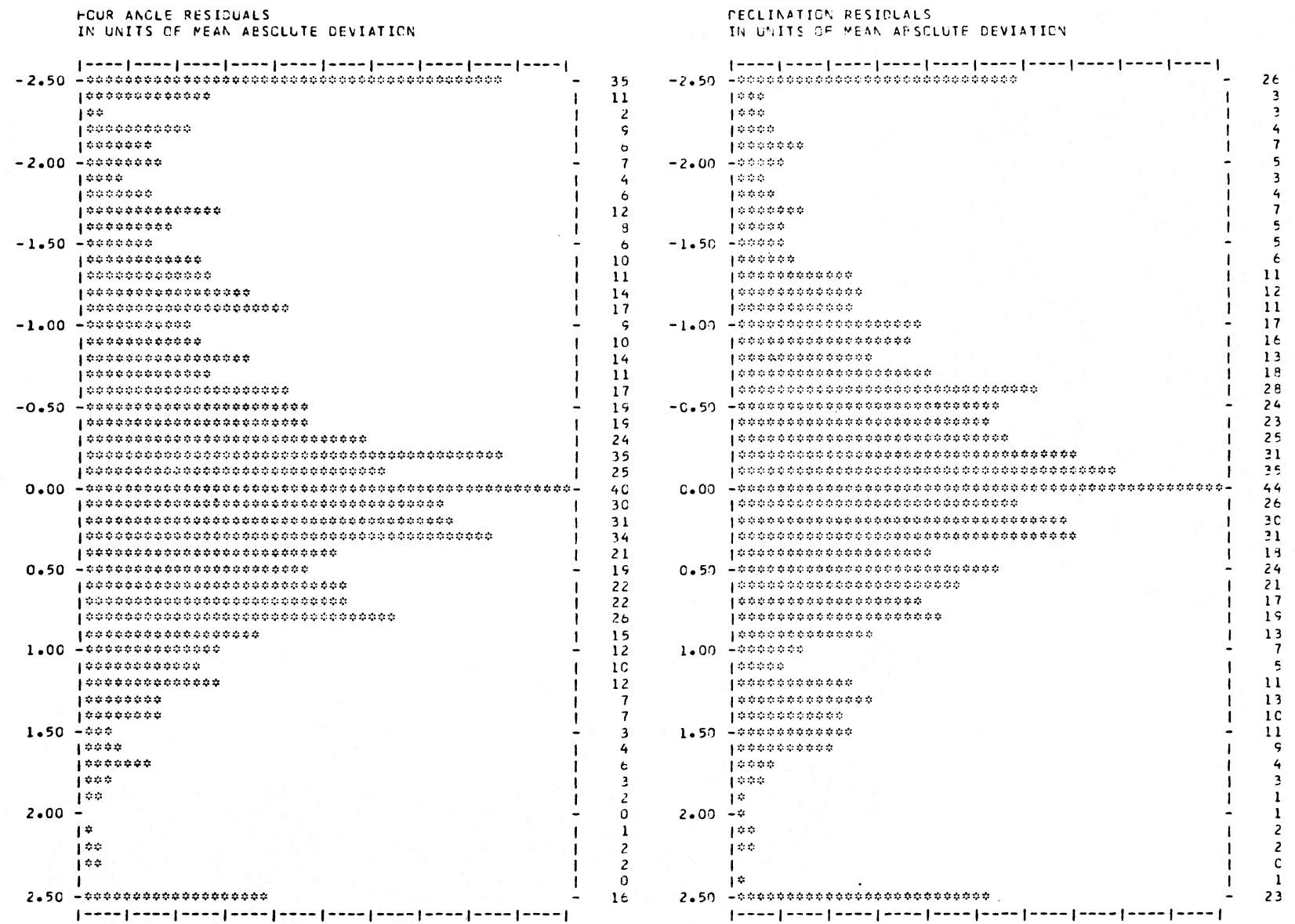
HOUR ANGLE RESIDUALS
IN UNITS OF MEAN ABSOLUTE DEVIATION
-2.50 35
11
2
9
6
-2.00 7
4
6
12
8
-1.50 6
10
11
14
17
-1.00 9
10
14
11
17
-0.50 19
19
24
35
25
0.00 40
30
31
34
21
0.50 19
22
22
26
15
1.00 12
10
12
7
7
1.50 3
4
6
3
2
2.00 0
1
2
2
0
2.50 16
DECLINATION RESIDUALS
IN UNITS OF MEAN ABSOLUTE DEVIATION
-2.50 26
3
3
4
7
-2.00 5
3
4
7
5
-1.50 5
6
11
12
11
-1.00 17
16
13
18
28
-0.50 24
23
25
31
35
0.00 44
26
30
31
18
0.50 24
21
17
19
13
1.00 7
5
11
13
10
1.50 11
9
4
3
1
2.00 1
2
2
0
1
2.50 23

FIGURE 1

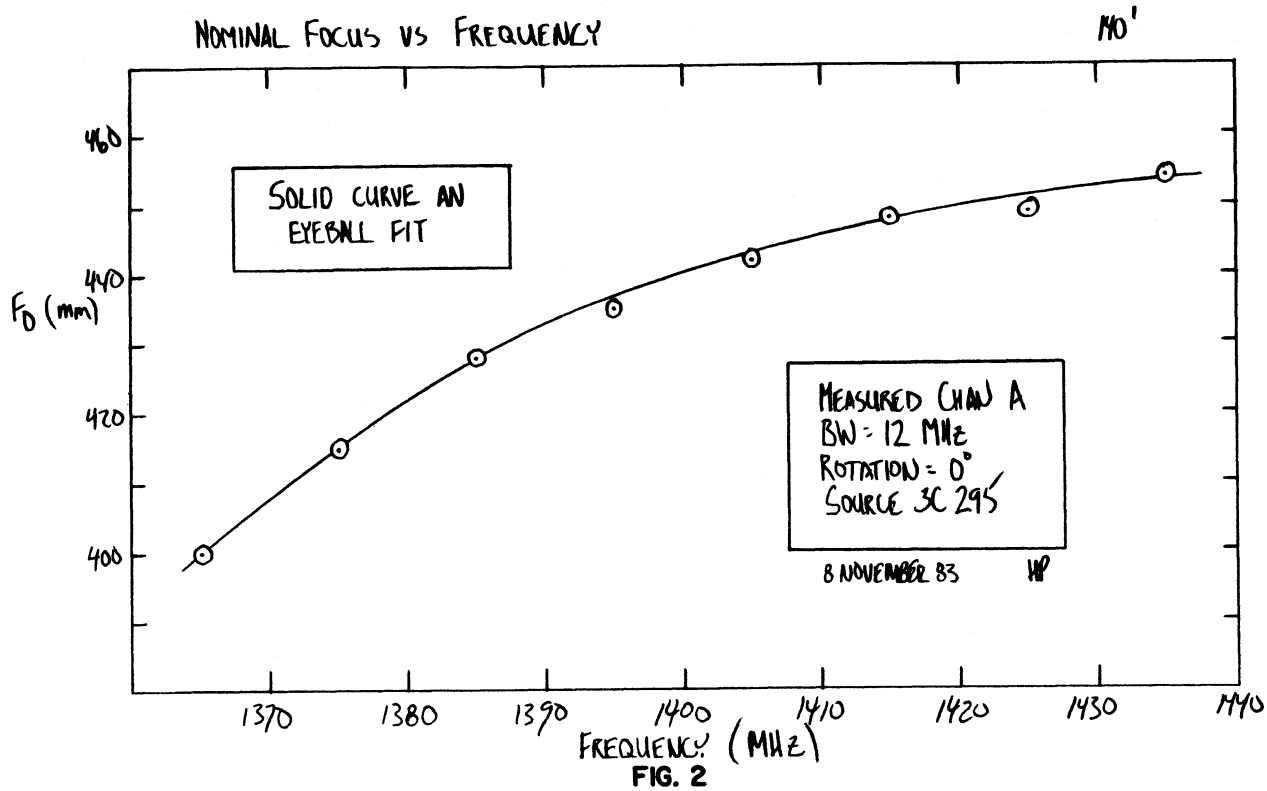
NOMINAL FOCUS VS FREQUENCY
140'
SOLID CURVE AN EYEBALL FIT
MEASURED CHAN A
BW = 12 MHz
ROTATION = 0°
SOURCE 3C 295
8 NOVEMBER 83 HP
F_D (mm)
460
440
420
400
1370
1380
1390
1400
1410
1420
1430
1440
FREQUENCY (MHz)

FIG. 2

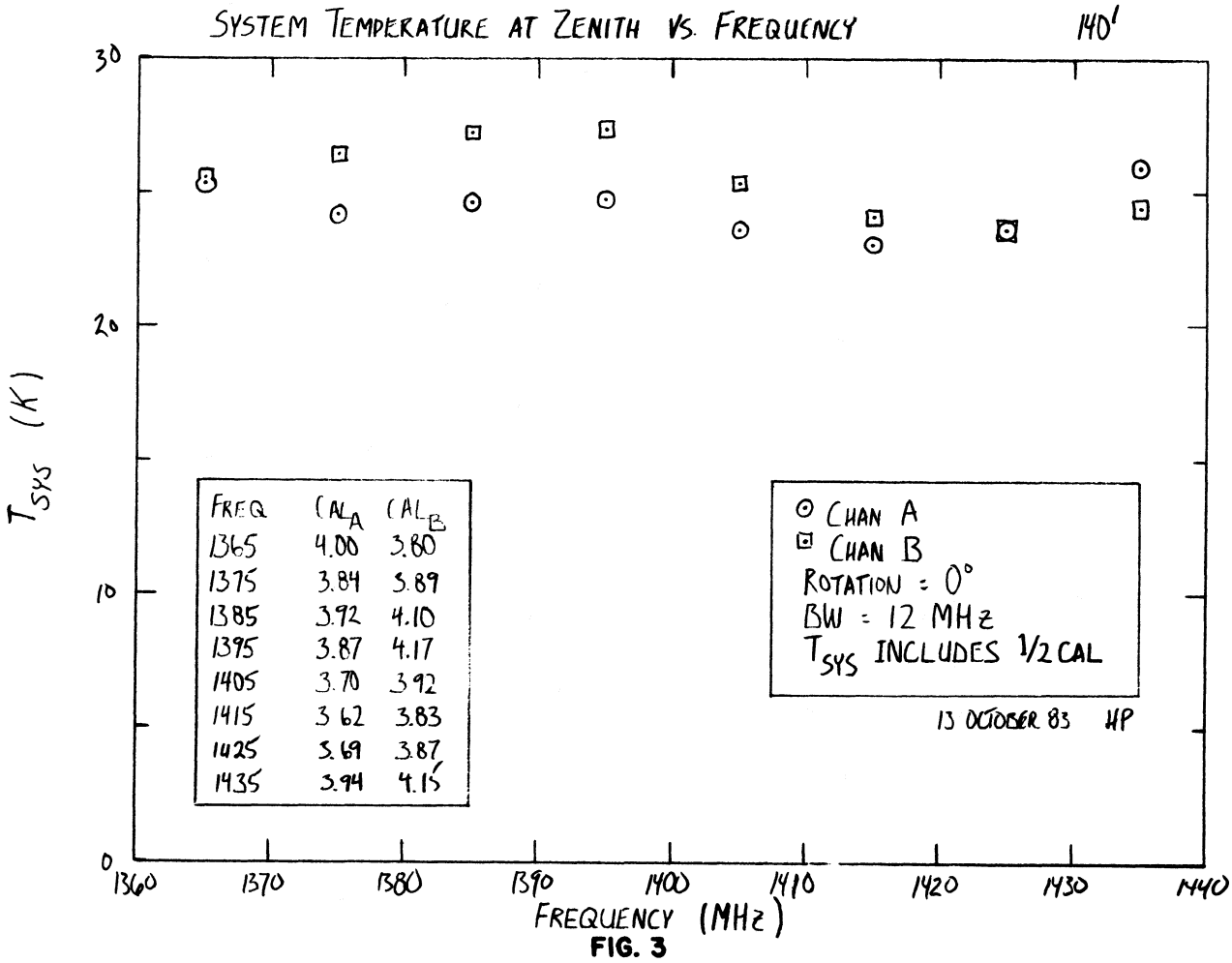
SYSTEM TEMPERATURE AT ZENITH VS. FREQUENCY
140'
T_{SYS} (K)
30
20
10
0
1360
1370
1380
1390
1400
1410
1420
1430
1440
FREQUENCY (MHz)
FREQ CAL$_A$ CAL$_B$
1365 4.00 3.80
1375 3.84 3.89
1385 3.92 4.10
1395 3.87 4.17
1405 3.70 3.92
1415 3.62 3.83
1425 3.69 3.87
1435 3.94 4.15
CHAN A
CHAN B
ROTATION = 0°
BW = 12 MHz
T_{SYS} INCLUDES 1/2 CAL
13 OCTOBER 83 HP

FIG. 3

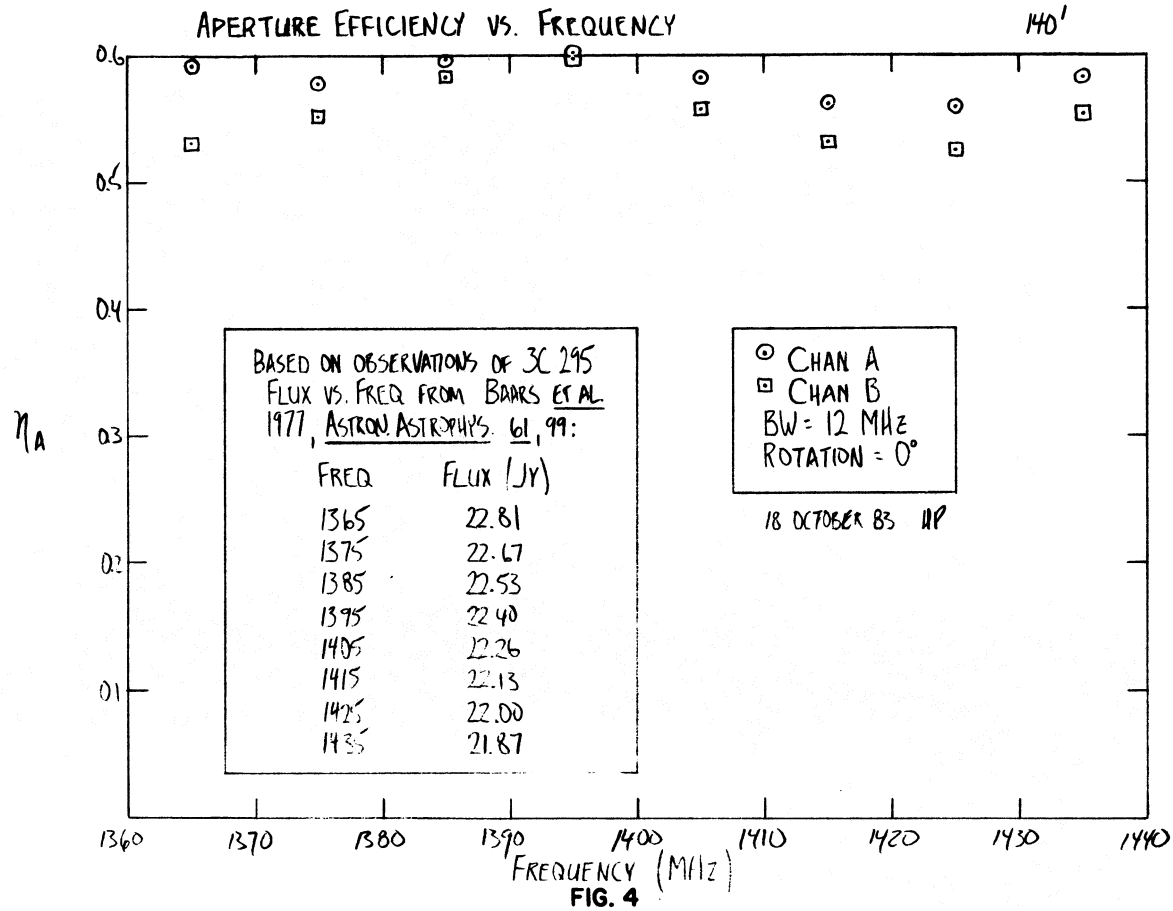
APERTURE EFFICIENCY VS. FREQUENCY
140'
0.6
0.5
0.4
0.3
0.2
0.1
η_A
BASED ON OBSERVATIONS OF 3C 295
FLUX VS. FREQ FROM BAARS ET AL.
1977, ASTRON. ASTROPHYS. 61, 99:
FREQ FLUX (JY)
1365 22.81
1375 22.67
1385 22.53
1395 22.40
1405 22.26
1415 22.13
1425 22.00
1435 21.87
⊙ CHAN A
⊡ CHAN B
BW = 12 MHz
ROTATION = 0°
18 OCTOBER 83 HP
1360
1370
1380
1390
1400
1410
1420
1430
1440
FREQUENCY (MHz)

FIG. 4

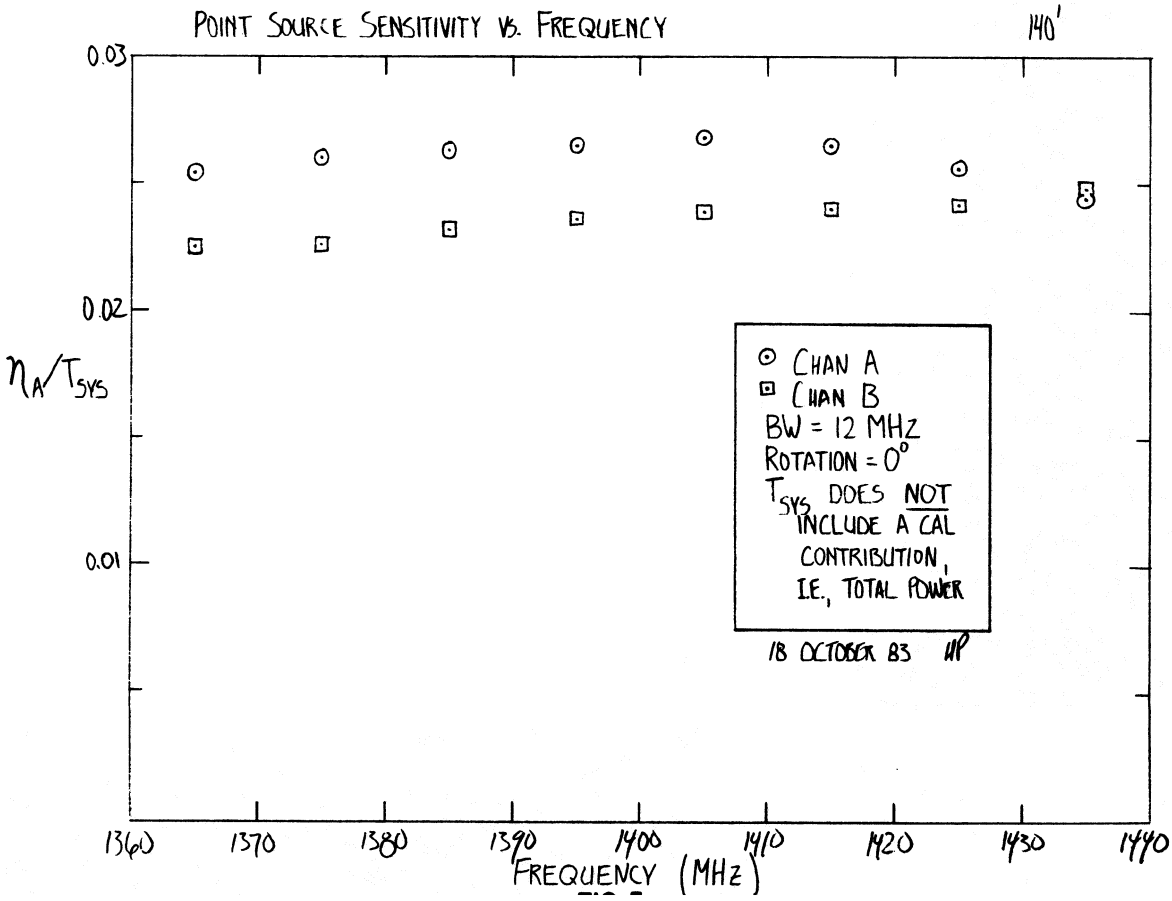
POINT SOURCE SENSITIVITY VS. FREQUENCY
140'
0.03
0.02
0.01
η_A/T_{SYS}
⊙ CHAN A
⊡ CHAN B
BW = 12 MHz
ROTATION = 0°
T_{SYS} DOES NOT INCLUDE A CAL CONTRIBUTION, I.E., TOTAL POWER
18 OCTOBER 83 HP
1360
1370
1380
1390
1400
1410
1420
1430
1440
FREQUENCY (MHz)

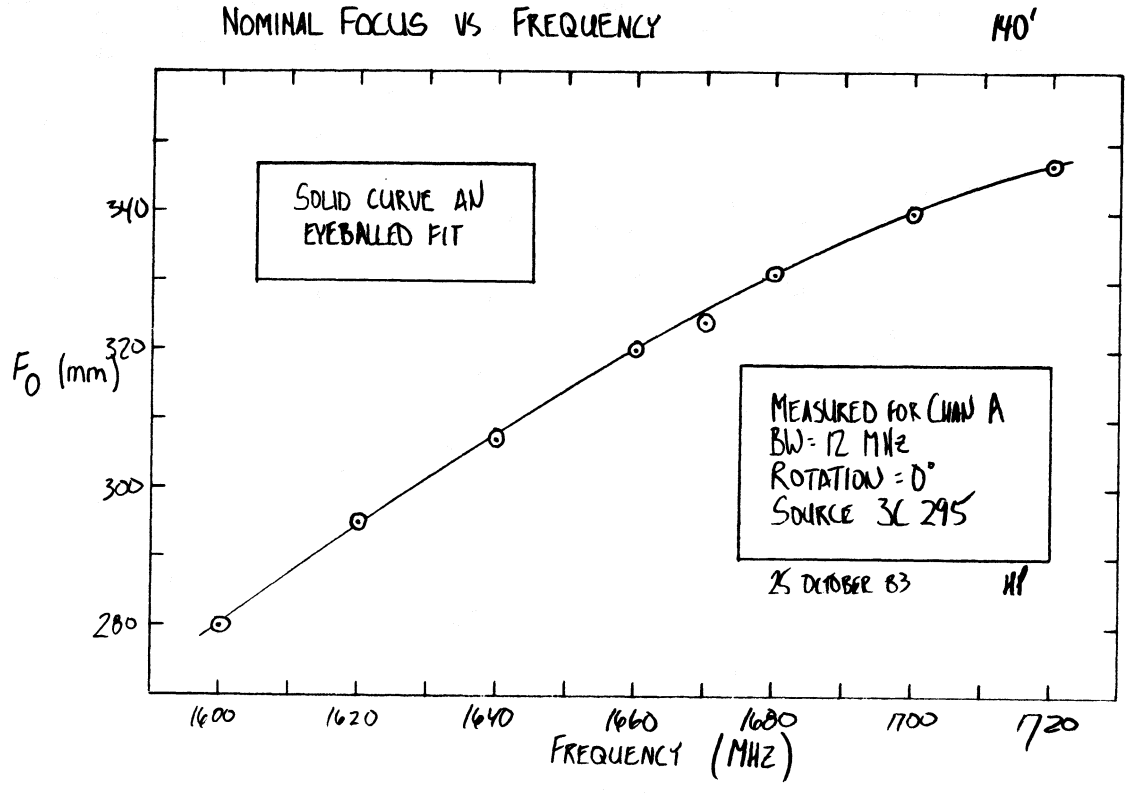
NOMINAL FOCUS VS FREQUENCY
140'
SOLID CURVE AN EYEBALLED FIT
MEASURED FOR CHAN A
BW = 12 MHz
ROTATION = 0°
SOURCE 3C 295
25 OCTOBER 83 HP
F_0 (mm)
340
320
300
280
1600
1620
1640
1660
1680
1700
1720
FREQUENCY (MHz)

FIG. 6

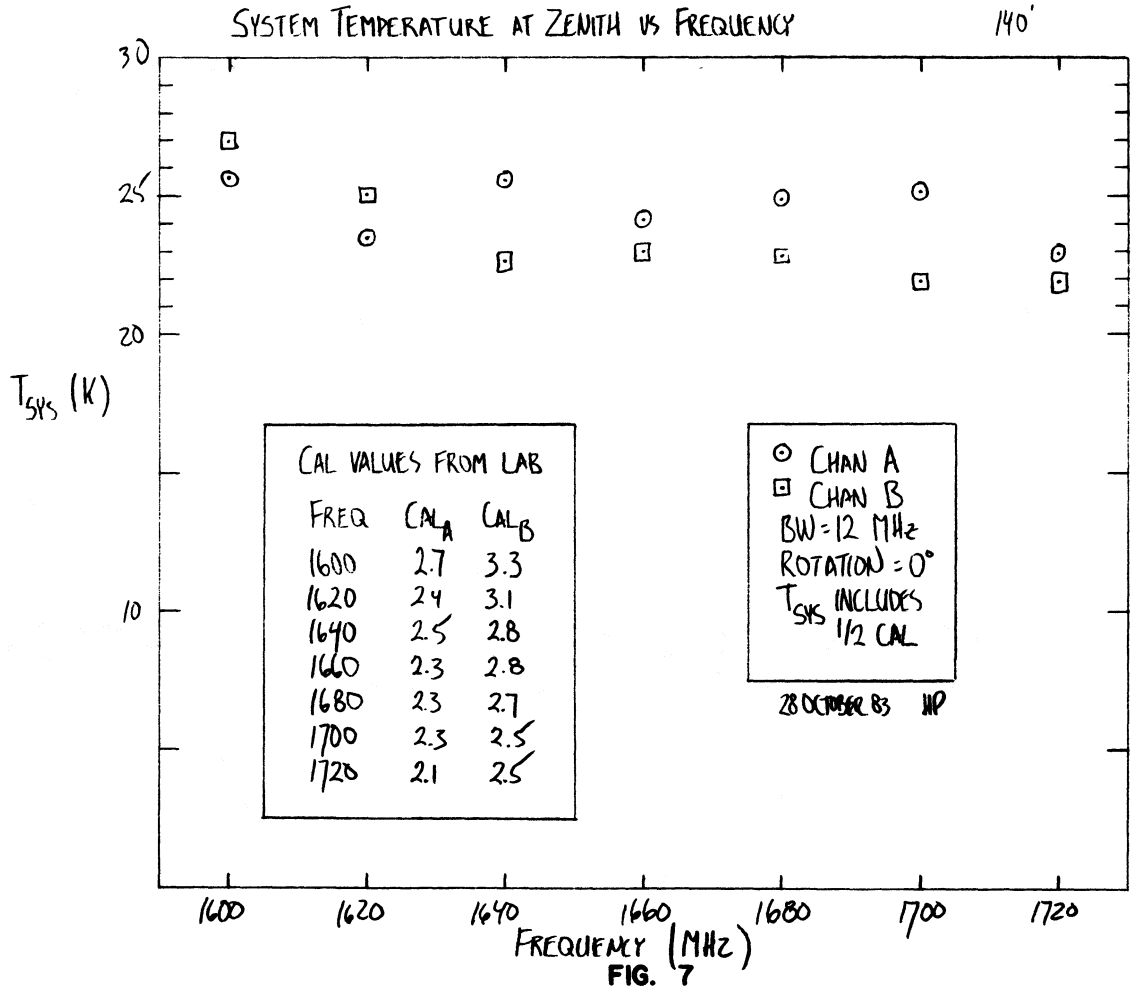
SYSTEM TEMPERATURE AT ZENITH VS FREQUENCY
140'
CAL VALUES FROM LAB
FREQ CAL$_A$ CAL$_B$
1600 2.7 3.3
1620 2.4 3.1
1640 2.5 2.8
1660 2.3 2.8
1680 2.3 2.7
1700 2.3 2.5
1720 2.1 2.5
⊙ CHAN A
⊡ CHAN B
BW = 12 MHz
ROTATION = 0°
T_{SYS} INCLUDES 1/2 CAL
28 OCTOBER 83 HP
T_{SYS} (K)
30
25
20
10
1600
1620
1640
1660
1680
1700
1720
FREQUENCY (MHz)

FIG. 7

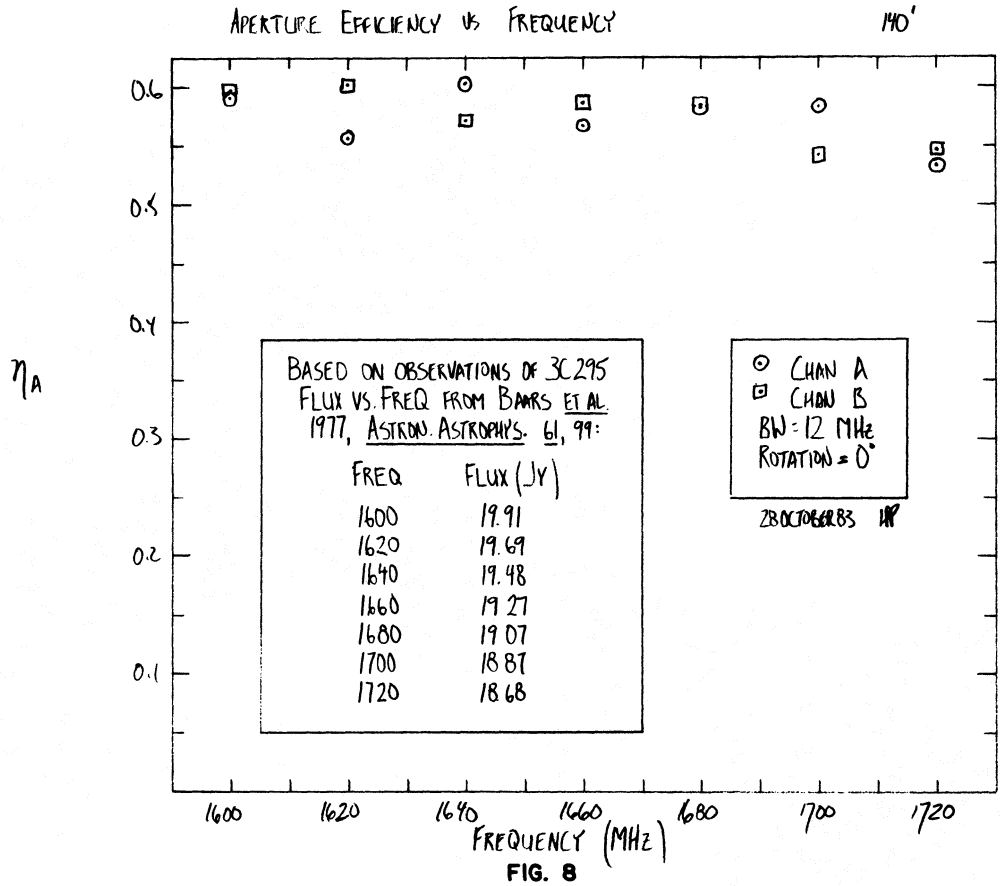
APERTURE EFFICIENCY VS FREQUENCY
140'
η_A
0.6
0.5
0.4
0.3
0.2
0.1
BASED ON OBSERVATIONS OF 3C295
FLUX VS. FREQ FROM BAARS ET AL.
1977, ASTRON. ASTROPHYS. 61, 99:
FREQ FLUX (JY)
1600 19.91
1620 19.69
1640 19.48
1660 19.27
1680 19.07
1700 18.87
1720 18.68
CHAN A
CHAN B
BW = 12 MHz
ROTATION = 0°
28 OCTOBER 83
1600
1620
1640
1660
1680
1700
1720
FREQUENCY (MHz)

FIG. 8

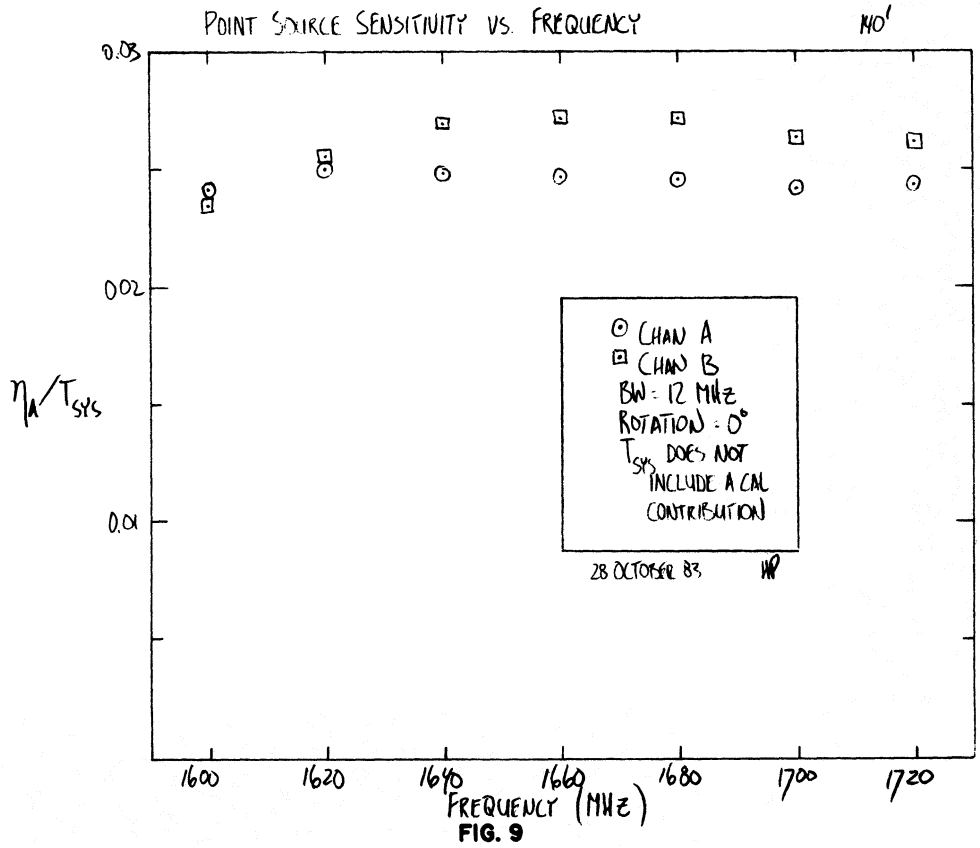
POINT SOURCE SENSITIVITY VS. FREQUENCY
140'
η_A/T_{SYS}
0.03
0.02
0.01
CHAN A
CHAN B
BW = 12 MHz
ROTATION = 0°
T_{SYS} DOES NOT INCLUDE A CAL CONTRIBUTION
28 OCTOBER 83
1600
1620
1640
1660
1680
1700
1720
FREQUENCY (MHz)

FIG. 9

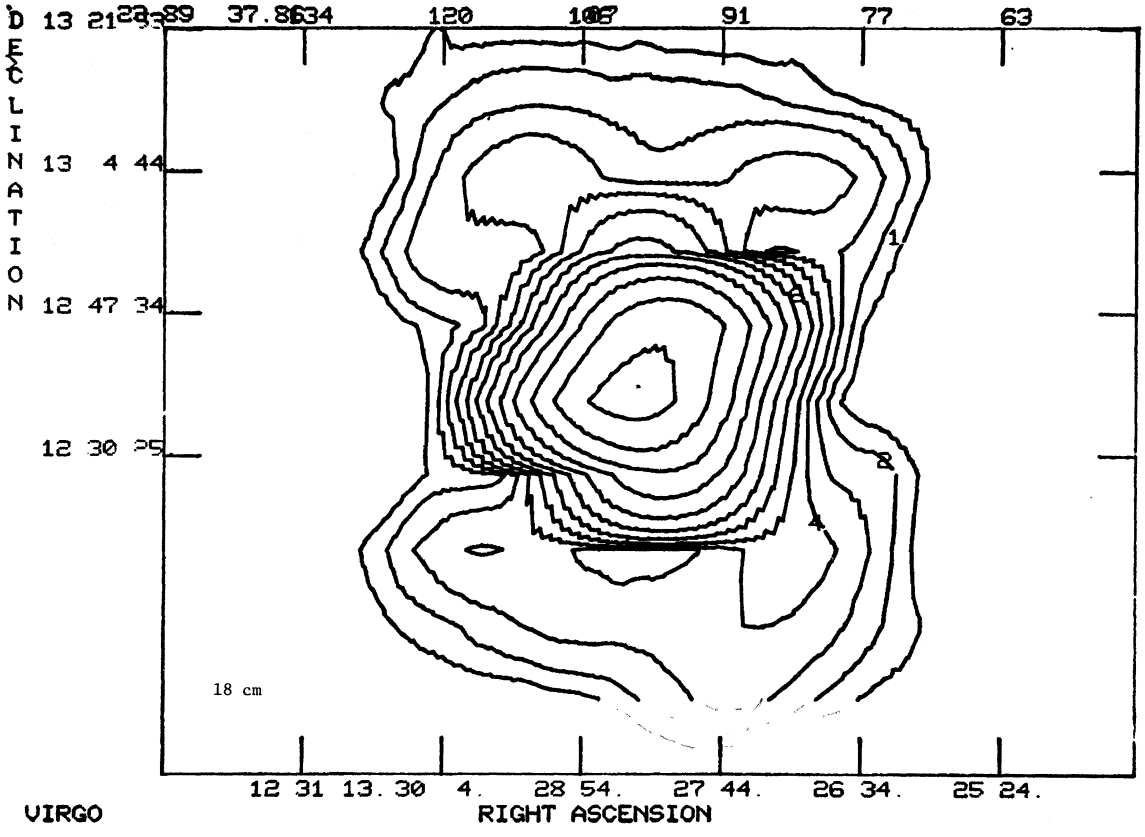

Channel A: 2 dB contours, lowest is -24 dB.

FIG. 10

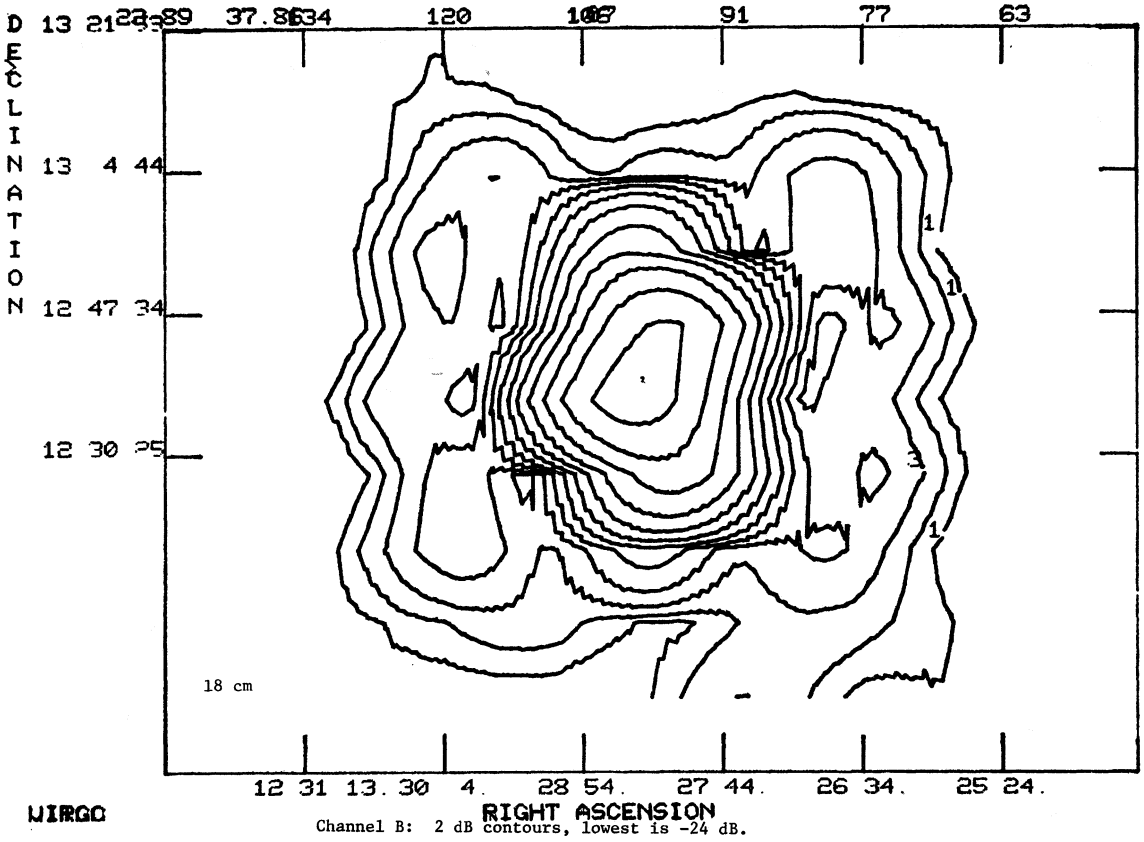

Channel B: 2 dB contours, lowest is -24 dB.

FIG. 11

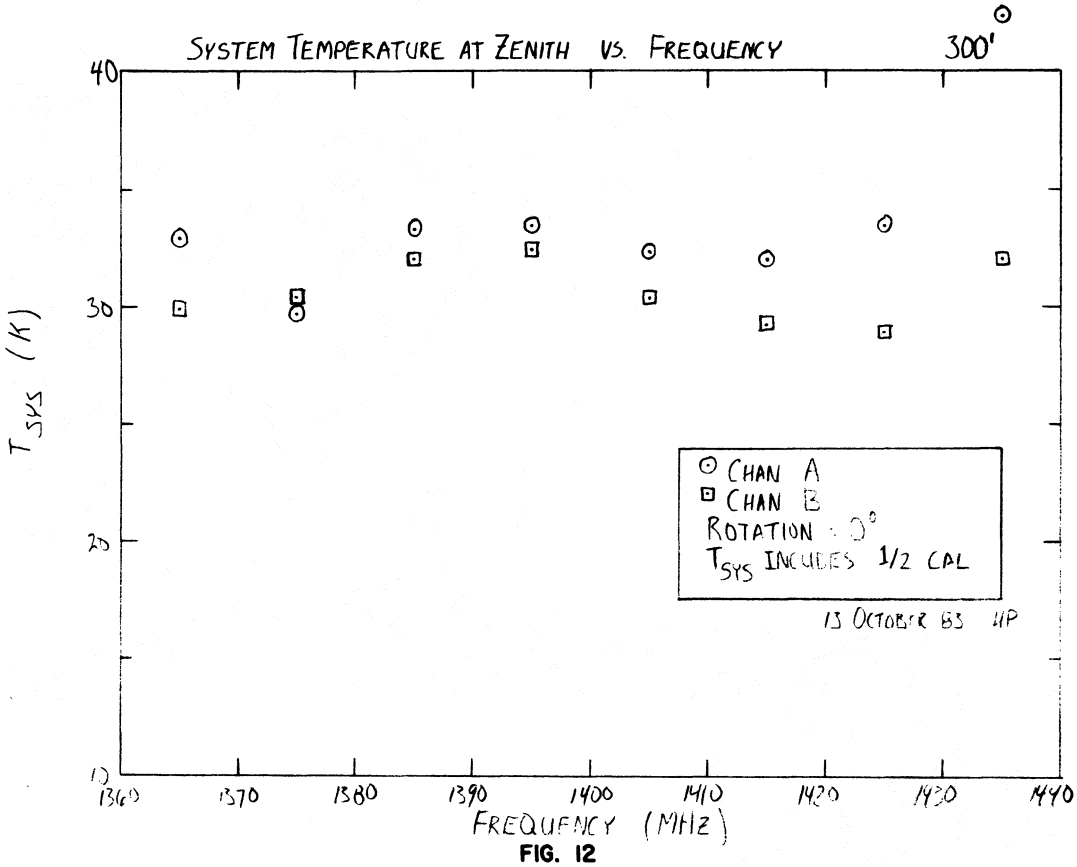
SYSTEM TEMPERATURE AT ZENITH VS. FREQUENCY
300'
40
30
20
10
T_{SYS} (K)
1360
1370
1380
1390
1400
1410
1420
1430
1440
FREQUENCY (MHZ)
CHAN A
CHAN B
ROTATION = 0°
T_{SYS} INCLUDES 1/2 CAL
13 OCTOBER 83 HP

FIG. 12

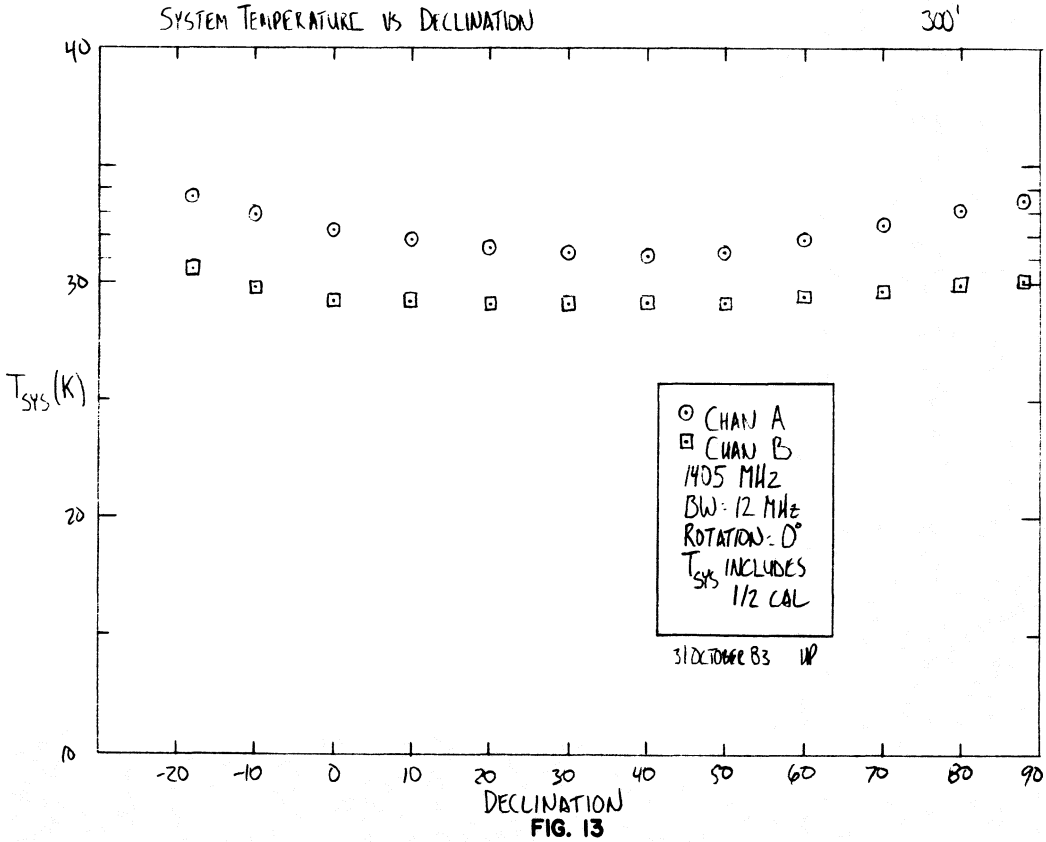
SYSTEM TEMPERATURE VS DECLINATION
300'
40
30
20
10
T_{SYS}(K)
-20
-10
0
10
20
30
40
50
60
70
80
90
DECLINATION
CHAN A
CHAN B
1405 MHz
BW = 12 MHz
ROTATION = 0°
T_{SYS} INCLUDES 1/2 CAL
31 OCTOBER 83 HP

FIG. 13

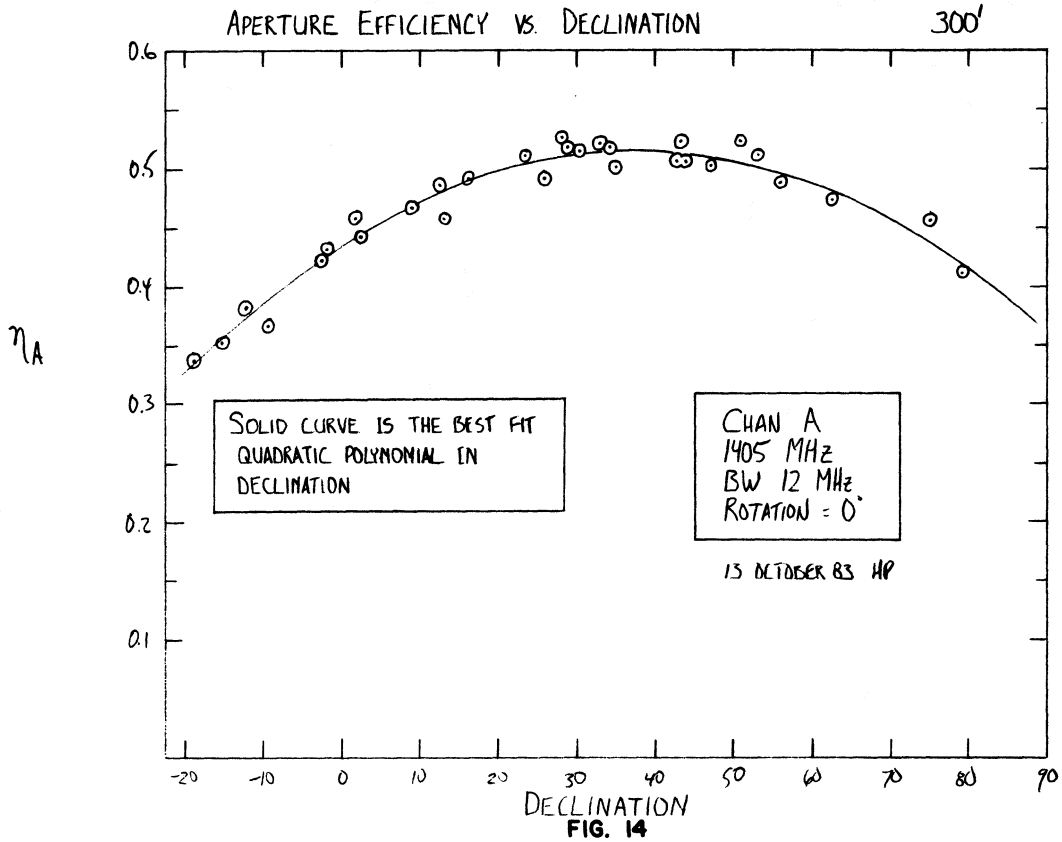
APERTURE EFFICIENCY VS. DECLINATION
300'
η_A
0.6
0.5
0.4
0.3
0.2
0.1
SOLID CURVE IS THE BEST FIT QUADRATIC POLYNOMIAL IN DECLINATION
CHAN A
1405 MHz
BW 12 MHz
ROTATION = 0°
13 OCTOBER 83 HP
-20 -10 0 10 20 30 40 50 60 70 80 90
DECLINATION

FIG. 14

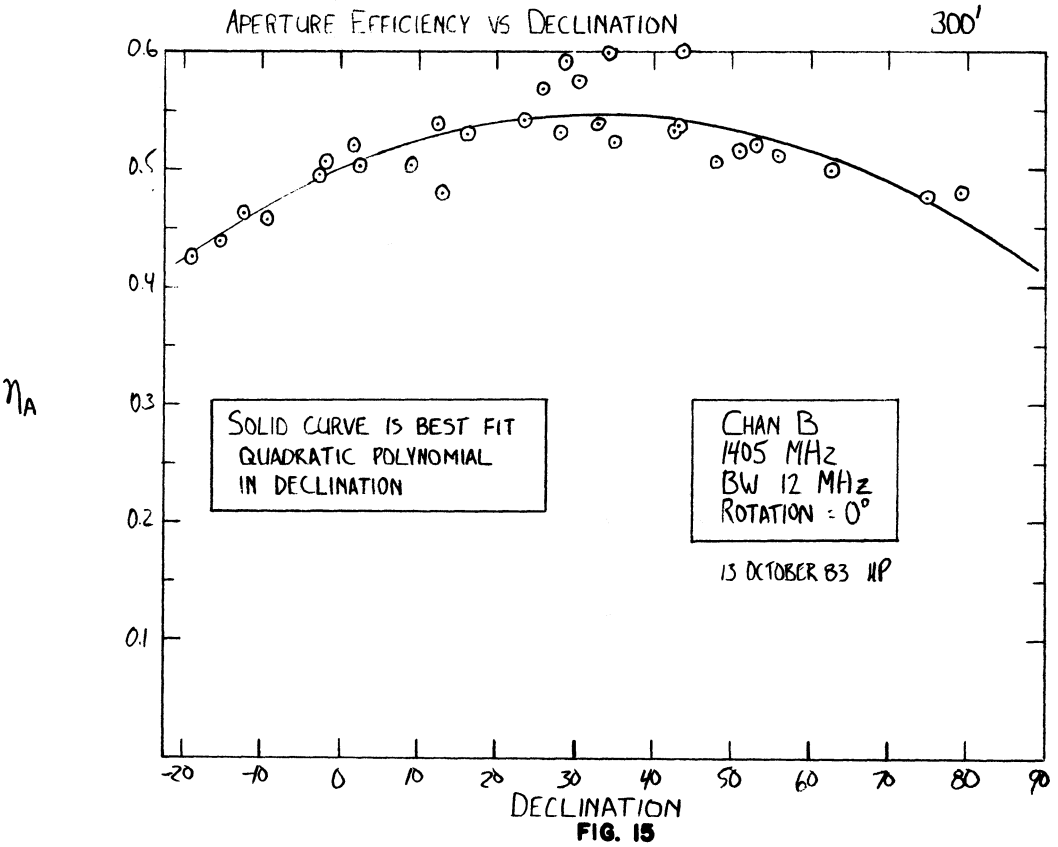
APERTURE EFFICIENCY VS DECLINATION
300'
η_A
0.6
0.5
0.4
0.3
0.2
0.1
SOLID CURVE IS BEST FIT QUADRATIC POLYNOMIAL IN DECLINATION
CHAN B
1405 MHz
BW 12 MHz
ROTATION = 0°
13 OCTOBER 83 HP
-20 -10 0 10 20 30 40 50 60 70 80 90
DECLINATION

FIG. 15

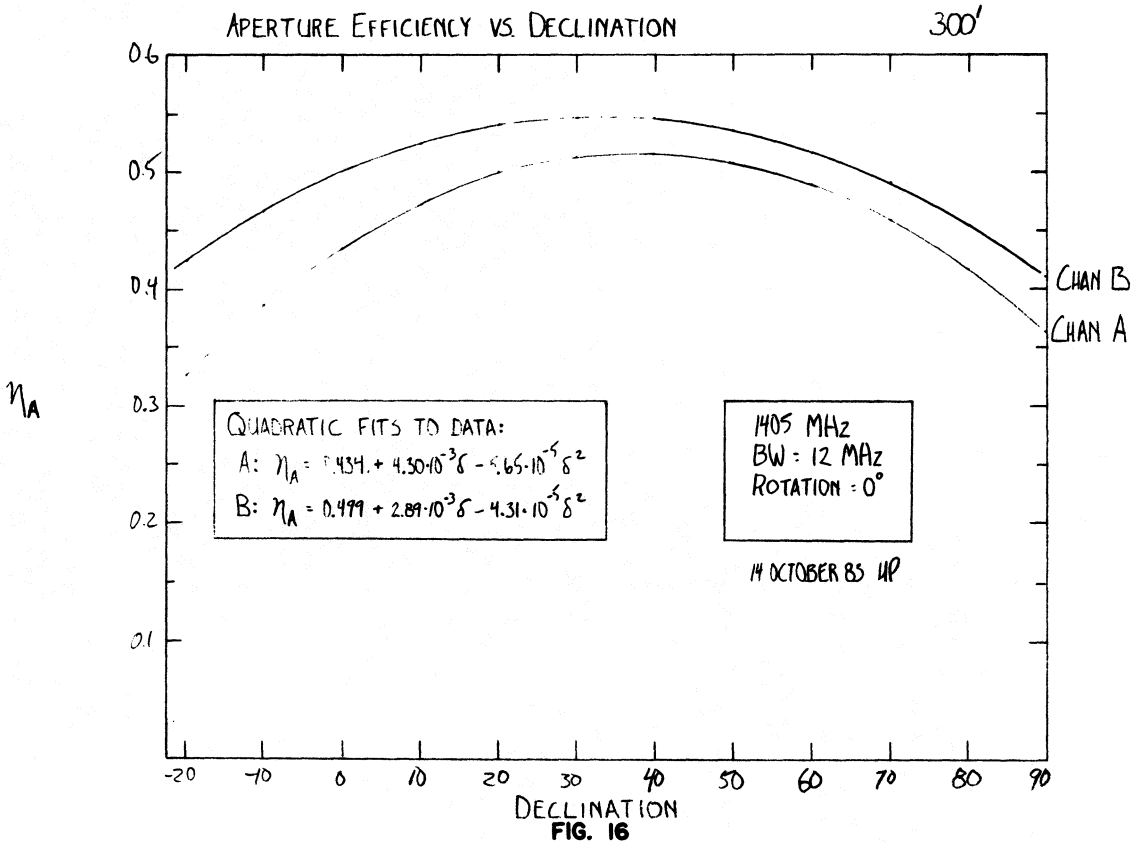
APERTURE EFFICIENCY VS. DECLINATION
300'
0.6
0.5
0.4
0.3
0.2
0.1
η_A
CHAN B
CHAN A
QUADRATIC FITS TO DATA:
A: $\eta_A = 0.434 + 4.30 \cdot 10^{-3}\delta - 5.65 \cdot 10^{-5}\delta^2$
B: $\eta_A = 0.499 + 2.89 \cdot 10^{-3}\delta - 4.31 \cdot 10^{-5}\delta^2$
1405 MHz
BW = 12 MHz
ROTATION = 0°
14 OCTOBER 83 HP
-20 -10 0 10 20 30 40 50 60 70 80 90
DECLINATION

FIG. 16

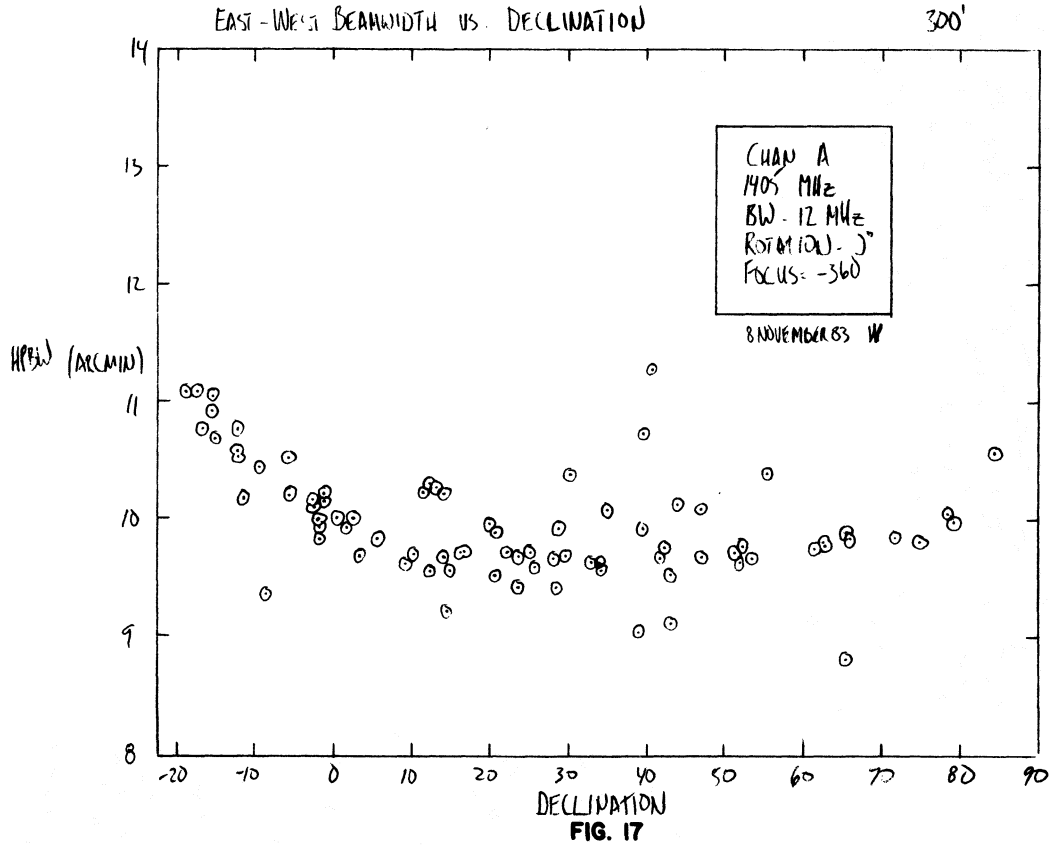
EAST-WEST BEAMWIDTH VS. DECLINATION
300'
14
13
12
11
10
9
8
HPBW (ARCMIN)
CHAN A
1405 MHz
BW = 12 MHz
ROTATION = 0°
FOCUS = -360
8 NOVEMBER 83 W
-20 -10 0 10 20 30 40 50 60 70 80 90
DECLINATION

FIG. 17

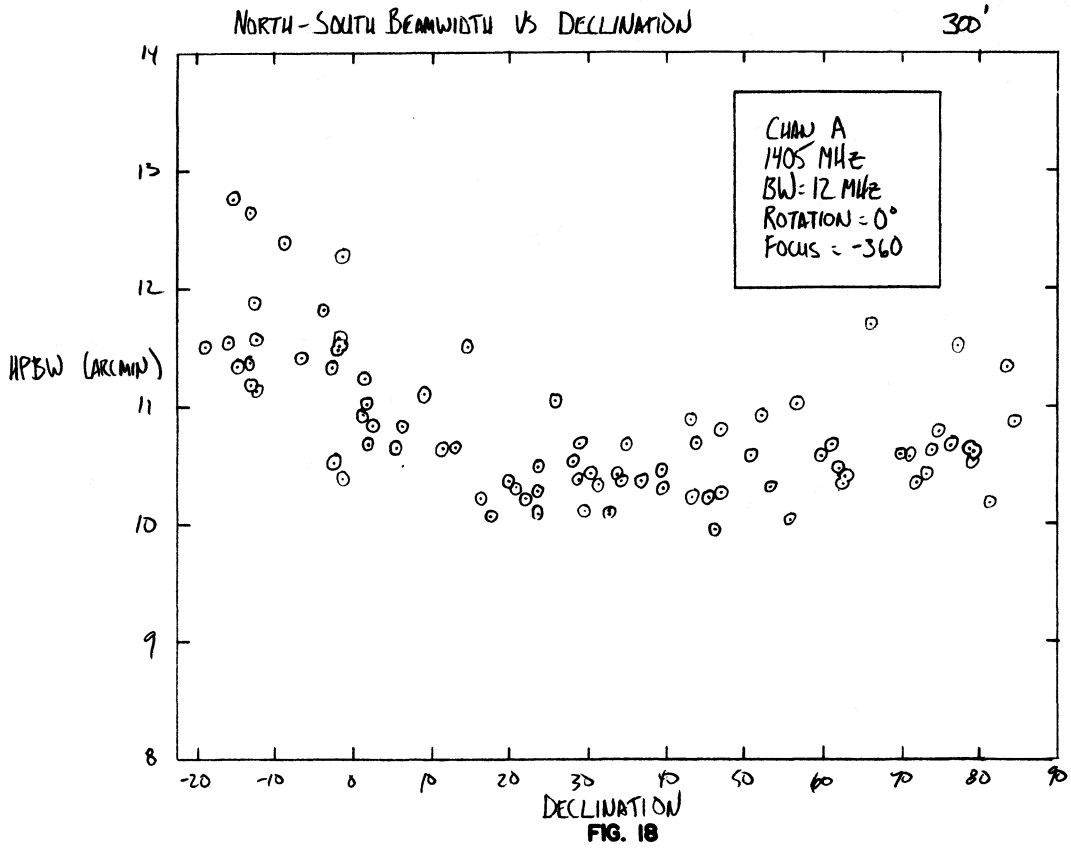
NORTH-SOUTH BEAMWIDTH VS DECLINATION
300'
CHAN A
1405 MHz
BW: 12 MHz
ROTATION: 0°
FOCUS: -360
HPBW (ARCMIN)
DECLINATION
14
13
12
11
10
9
8
-20
-10
0
10
20
30
40
50
60
70
80
90

FIG. 18

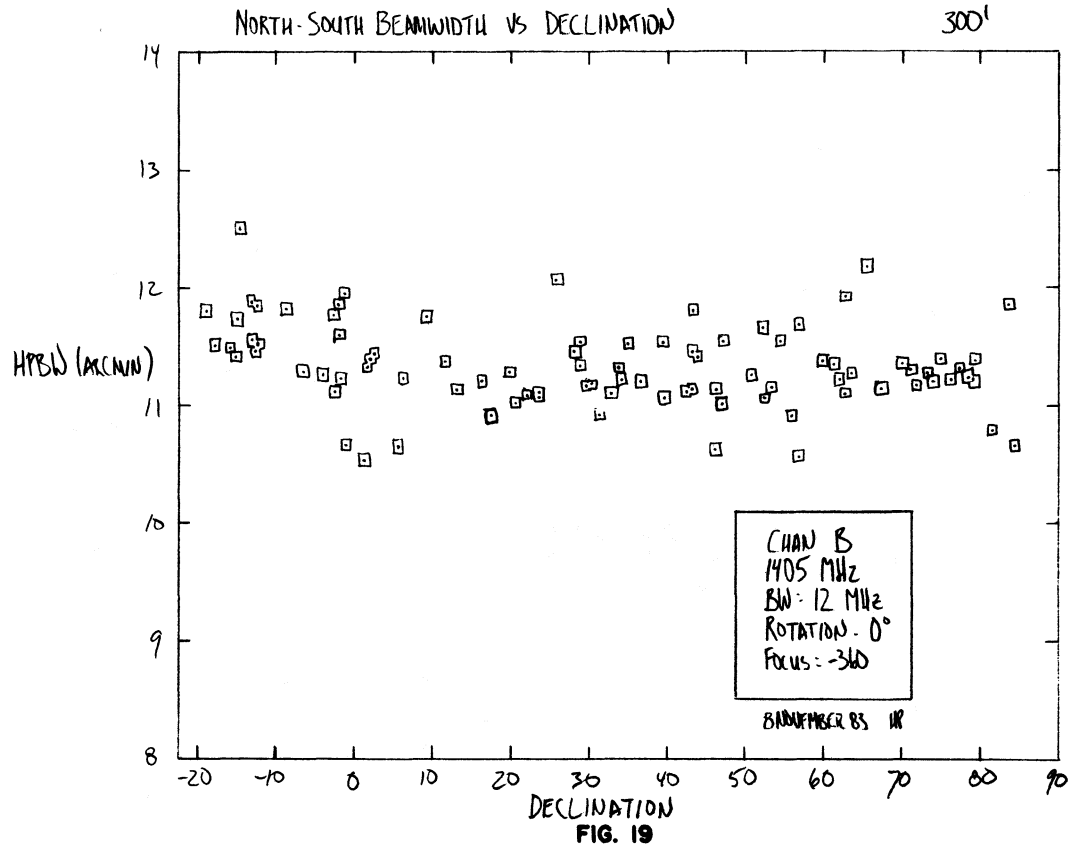
NORTH-SOUTH BEAMWIDTH VS DECLINATION
300'
CHAN B
1405 MHz
BW: 12 MHz
ROTATION: 0°
FOCUS: -360
HPBW (ARCMIN)
DECLINATION
14
13
12
11
10
9
8
-20
-10
0
10
20
30
40
50
60
70
80
90

FIG. 19

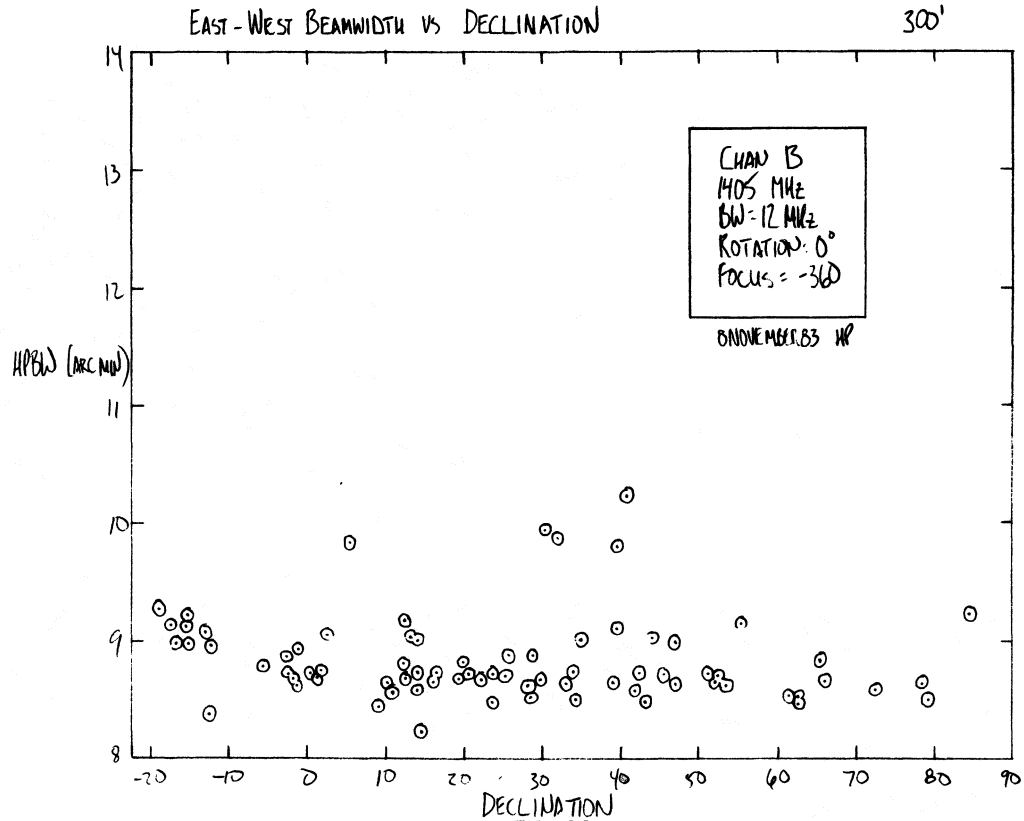
EAST-WEST BEAMWIDTH VS DECLINATION
300'
CHAN B
1405 MHz
BW = 12 MHz
ROTATION: 0°
FOCUS = -360
8 NOVEMBER 83 HP
HPBW (ARC MIN)
DECLINATION
14
13
12
11
10
9
8
-20
-10
0
10
20
30
40
50
60
70
80
90

FIG. 20

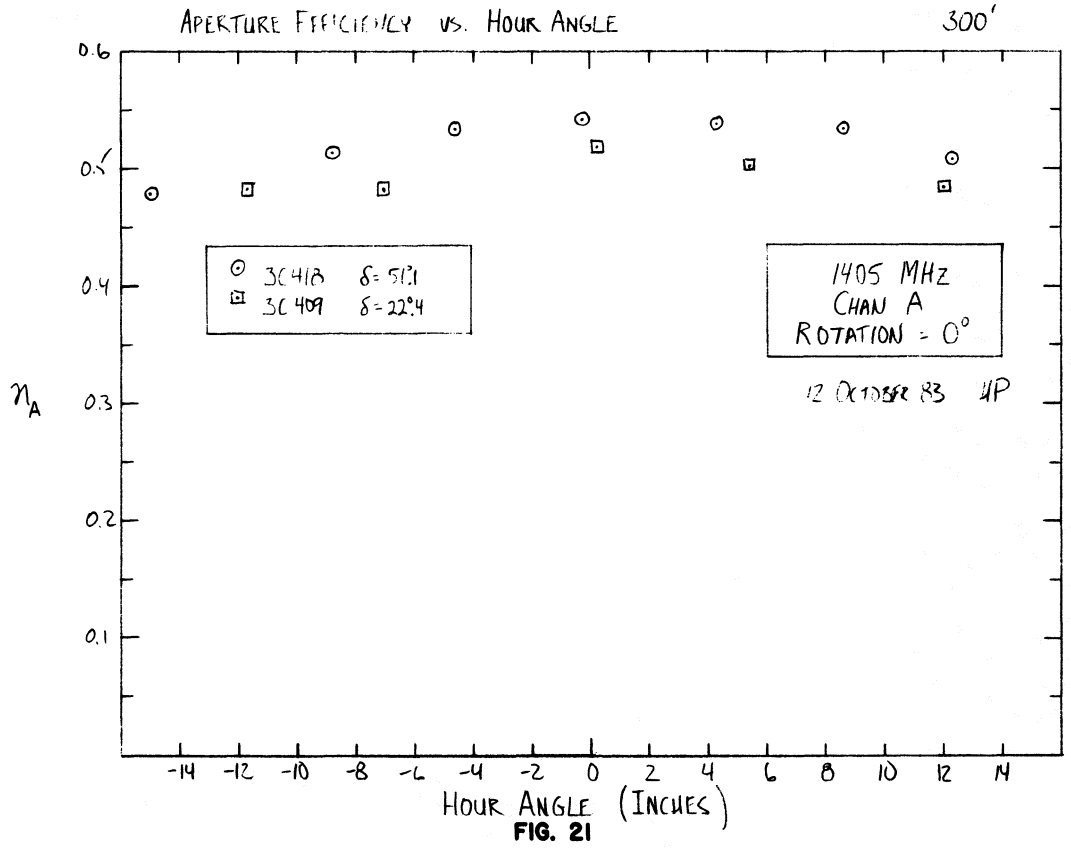
APERTURE EFFICIENCY VS. HOUR ANGLE
300'
3C 418 δ = 51.1
3C 409 δ = 22.4
1405 MHz
CHAN A
ROTATION = 0°
12 OCTOBER 83 HP
η_A
HOUR ANGLE (INCHES)
0.6
0.5
0.4
0.3
0.2
0.1
-14
-12
-10
-8
-6
-4
-2
0
2
4
6
8
10
12
14

FIG. 21

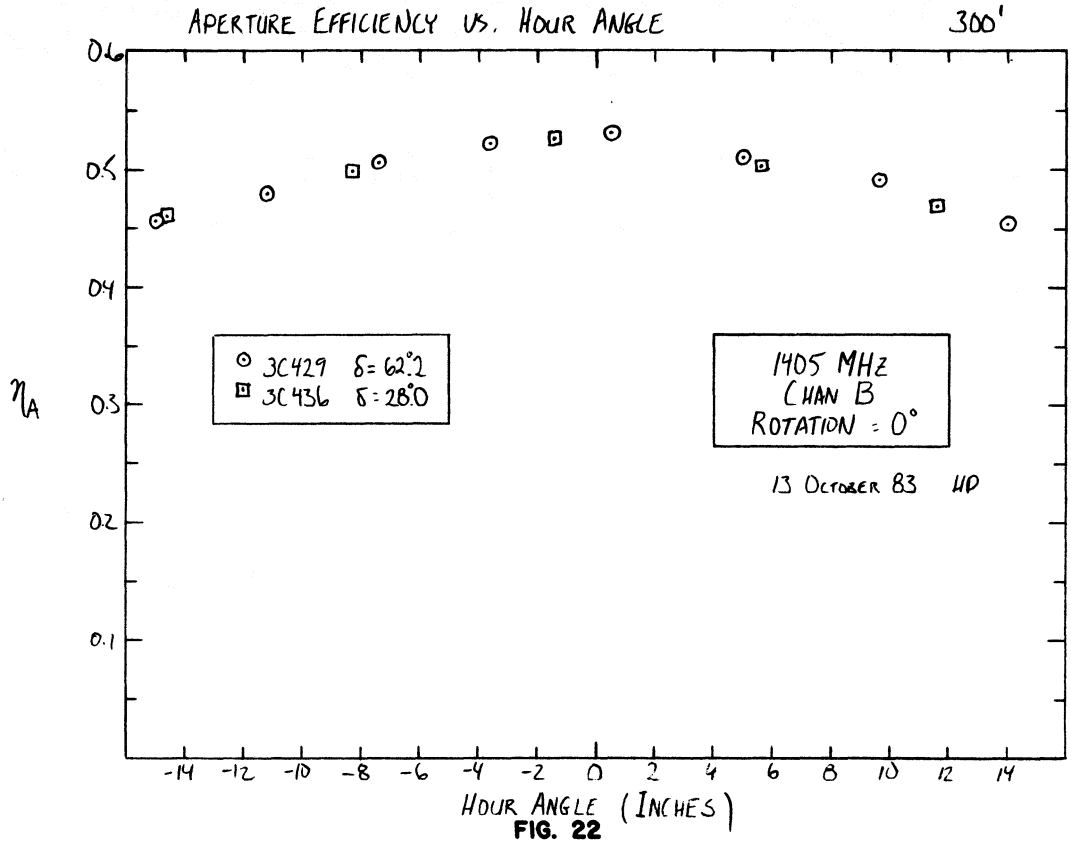

FIG. 22

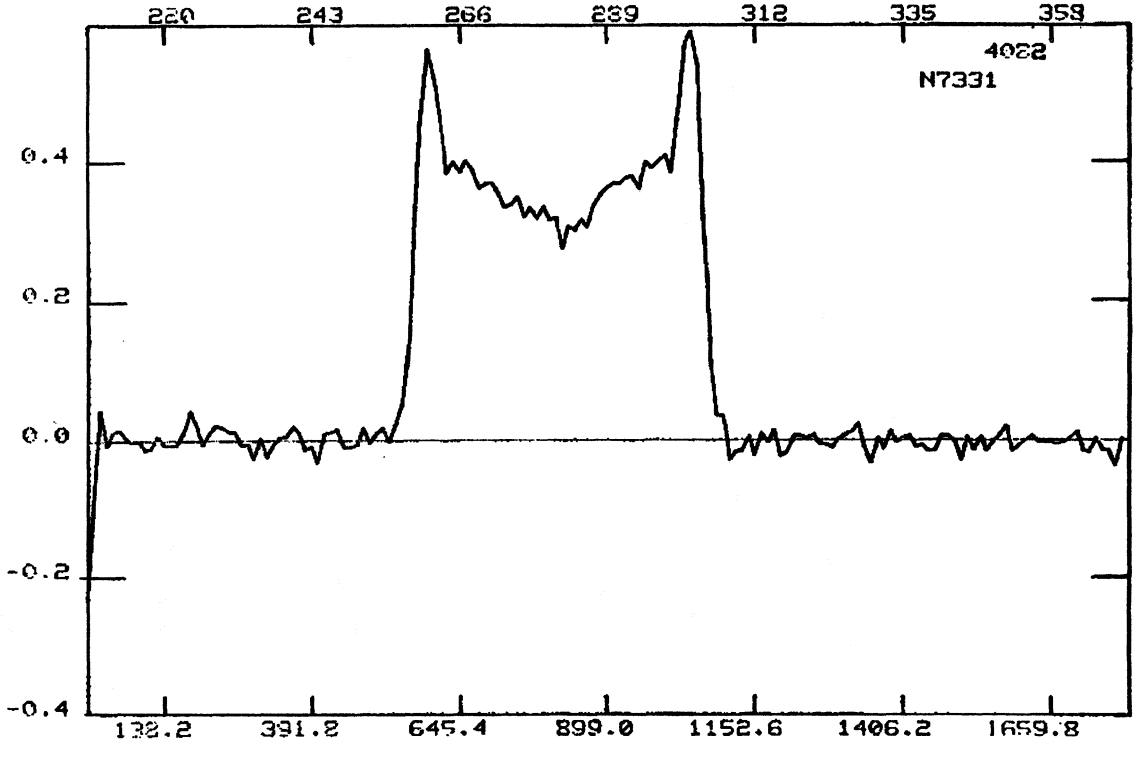

AVERAGE OF TWO OFFS, TWO RECEIBERS, LINEAR BASELINE

FIG. 23

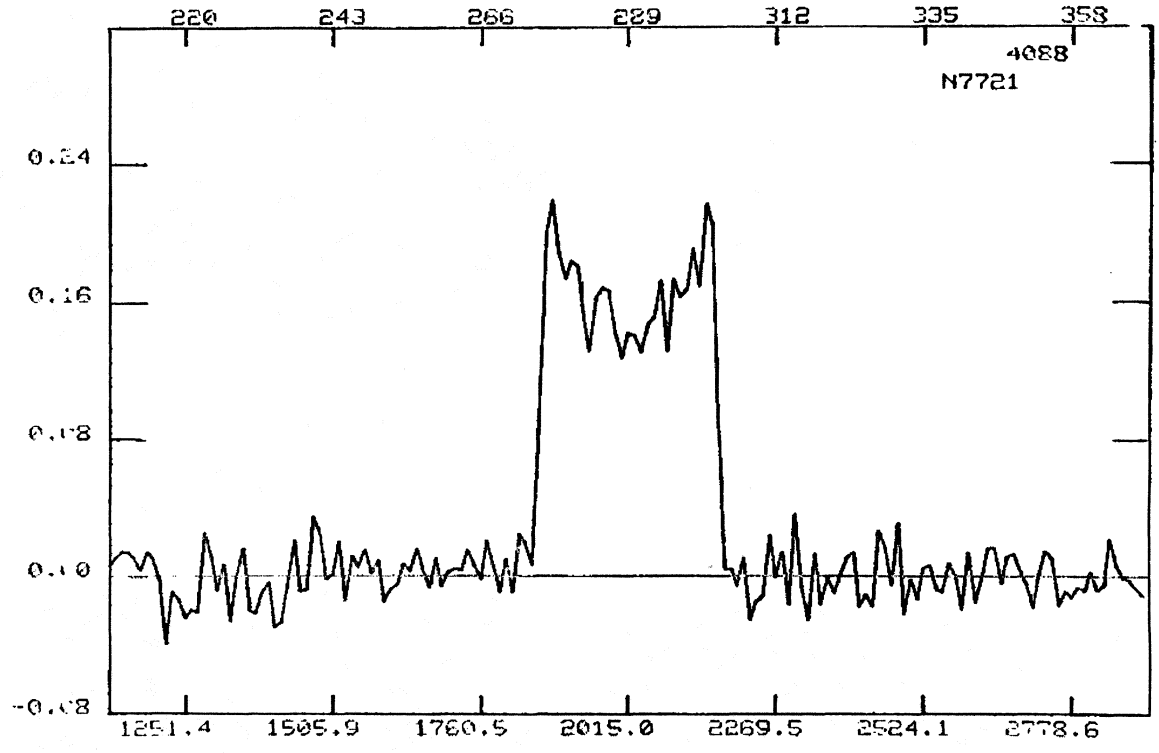

AVERAGE OF TWO OFFS, AVERAGE OF TWO RECEIVERS, LINEAR BASELINE

FIG. 24

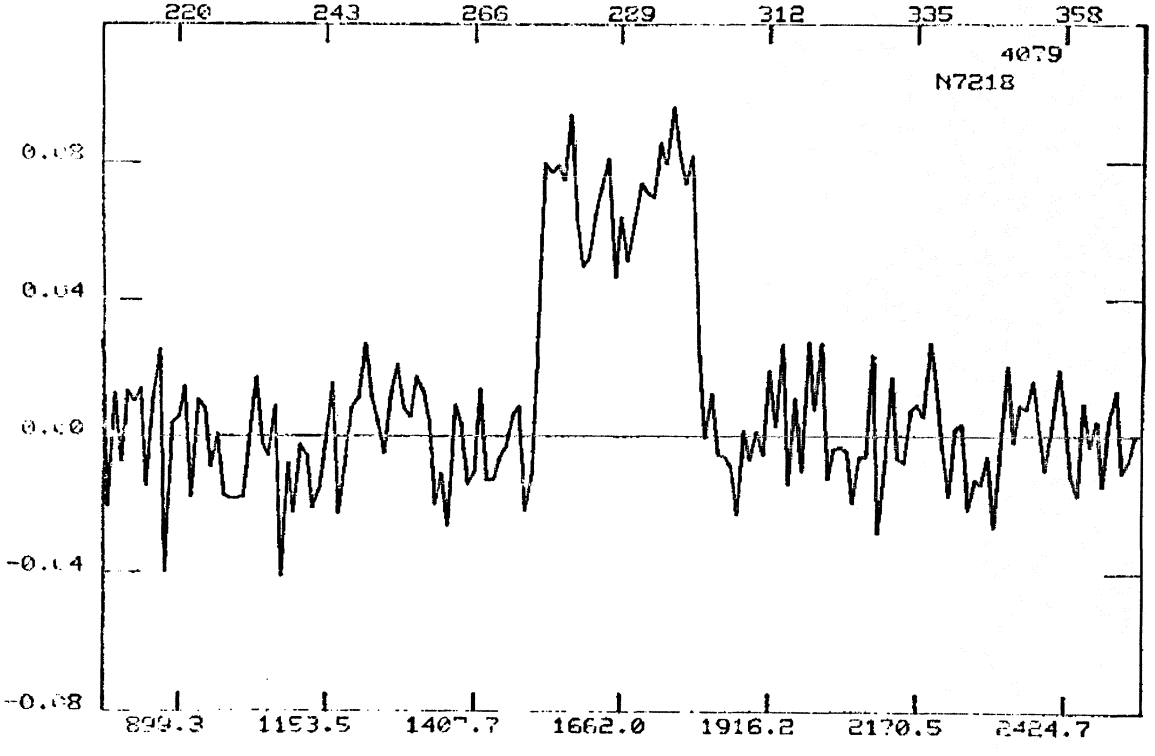

AVERAGE OF TWO OFFS, TWO RECEIVERS, LINEAR BASELINE

FIG. 25